REPORT DOCUMENTATION PAGE

AFRL-SR-AR-TR-04-

0540

The public reporting burden for this collection of information is estimated to average 1 hour per response, including gathering and maintaining the data needed, and completing and reviewing the collection of information. Send comments information, including suggestions for reducing the burden, to Department of Defense, Washington Headquarters Servi 1215 Jefferson Davis Highway, Suite 1204, Arlington, VA 22202-4302. Respondents should be aware that notwith| penalty for failing to comply with a collection of information if it does not display a currently valid OMB control number.
PLEASE DO NOT RETURN YOUR FORM TO THE ABOVE ADDRESS.

1. REPORT DATE *(DD-MM-YYYY)*	2. REPORT TYPE	3. DATES COVERED *(From - To)*
	Final	1 June 2001 - 30 June 2004

4. TITLE AND SUBTITLE	5a. CONTRACT NUMBER
Numerical Computation in MagnetoFluid Dynamics	
	5b. GRANT NUMBER
	F49620-01-1-0390
	5c. PROGRAM ELEMENT NUMBER

6. AUTHOR(S)	5d. PROJECT NUMBER
R. W. MacCormack	
	5e. TASK NUMBER
	5f. WORK UNIT NUMBER

7. PERFORMING ORGANIZATION NAME(S) AND ADDRESS(ES)	8. PERFORMING ORGANIZATION REPORT NUMBER
Department of Aeronautics and Astronautics Stanford University Stanford, CA 94305-4035	

9. SPONSORING/MONITORING AGENCY NAME(S) AND ADDRESS(ES)	10. SPONSOR/MONITOR'S ACRONYM(S)
Air Force Office of Scientific Research 4015 Wilson Blvd Mail Room 713 Arlington, VA 22203	AFOSR
	11. SPONSOR/MONITOR'S REPORT NUMBER(S)

12. DISTRIBUTION/AVAILABILITY STATEMENT

Distribution Statement A. Approved for public release; distribution is unlimited.

13. SUPPLEMENTARY NOTES

20041028 039

14. ABSTRACT

During the years supported by the subject AFOSR grant the following research accomplishments were made. Inclusion of both thermal and chemical non-equilibrium into the MFD equations. Simulation of the flow within MFD generators and accelerators for the proposed energy "bypass scram jet engine" concept. Reformulating the governing MFD equations for strong imposed magnetic fields, of the order of 10 Tesla, using the properties of the imposed magnetic fields, $V \cdot B = 0$ and $V \times B = 0$, to avoid products of the order of B^2 from dwarfing values of static fluid pressure. Analysis of the physics of upstream influence caused by magnetic diffusion and the eigenvalue properties of the MFD equations in comparison with the simpler "low magnetic Reynolds Number" approach for flows within MFD generators and accelerators. Analysis of non-uniqueness of the equations of magneto-fluid dynamics Inclusion of Cesium seeding into the flow and the Park model for calculating electrical conductivity based upon electron and ion concentrations. Analysis of the physics of upstream influence of the flow about the nose of a hypersonic vehicle.

15. SUBJECT TERMS

16. SECURITY CLASSIFICATION OF:			17. LIMITATION OF ABSTRACT	18. NUMBER OF PAGES	19a. NAME OF RESPONSIBLE PERSON
a. REPORT	b. ABSTRACT	c. THIS PAGE			R. W. MacCormack
U	U	U	UU		19b. TELEPHONE NUMBER *(Include area code)*

Standard Form 298 (Rev. 8/98)
Prescribed by ANSI Std. Z39.18

Final Performance Report

Grant: F49620-01-1-0390-P00003

Title: <u>Numerical Computation in MagnetoFluid-Dynamics</u>

Principal Investigator: <u>Robert W. MacCormack</u>

    Commercial Phone: <u>650-723-4627</u> FAX: <u>650-725-3377</u>

    Mailing Address: <u>Department of Aeronautics and Astronautics</u>
                           <u>Stanford University</u>
                           <u>Stanford, CA 94305-4035</u>
    E-Mail Address: <u>rwmacc@aol.com</u>

AFOSR Program Manager: <u>Dr. Fariba Fahroo</u>

Research Objectives:
a) Develop algorithms and boundary condition procedures for solving the complete equations governing magneto-fluid-dynamics
b) Apply the developed numerical procedures to simulate the flow about realistic aerospace configurations of Air Force interest
c) Support and complement magneto-fluid-dynamic research studies at AFRL

Status of Effort:
Prior to the start of the subject grant the following research accomplishments were made by the principal investigator toward flow simulation governed by the equations of magneto-fluid-dynamics.

(1) Reforming the flux vectors of the equations governing MFD to be "homogeneous of degree one" so that $F = AU$ and a flux split algorithm could de devised. $F_+ = A_+U$ and $F_- = A_-U$

(2) Simulation of the flow about the fore-body of a hypersonic vehicle and the calculation of drag and heat transfer with and without magnetic field interaction.

(3) Splitting the flux vectors directly, instead of basing the splitting on the state vector U. $F_+ = A_+A^{-1}F$ and $F_- = A_-A^{-1}F$

During the years supported by the subject AFOSR grant the following research accomplishments were made.

(4) Inclusion of both thermal and chemical non-equilibrium into the MFD equations.

(5) Simulation of the flow within MFD generators and accelerators for the proposed energy "bypass scram jet engine" concept.

(6) Reformulating the governing MFD equations for strong imposed magnetic fields, of the order of 10 Tesla, using the properties of the imposed magnetic fields, $\vec{\nabla}\cdot\vec{B} = 0$ and $\vec{\nabla}\times\vec{B} = 0$, to avoid products of the order of B^2 from dwarfing values of static fluid pressure.

(7) Analysis of the physics of upstream influence caused by magnetic diffusion and the eigenvalue properties of the MFD equations in comparison with the simpler "low magnetic Reynolds Number" approach for flows within MFD generators and accelerators.

(8) Analysis of non-uniqueness of the equations of magneto-fluid dynamics

(9) Inclusion of Cesium seeding into the flow and the Park model for calculating electrical conductivity based upon electron and ion concentrations.

(10) Analysis of the physics of upstream influence of the flow about the nose of a hypersonic vehicle

Accomplishments/New Findings:
Items (4), (6), (8) and (9) above represent progress toward research objective (a), Items (5) and (10) toward research objective (b) and Items (7) and (10) toward research objective (c). Each will be discussed below. First, we present the governing equations of magneto-fluid dynamics.

1. The Equations of Magneto-Fluid-Dynamics -
The unsteady equations of compressible viscous flow within an imposed magnetic field become

$$\frac{\partial U}{\partial t} + \frac{\partial F}{\partial x} + \frac{\partial G}{\partial y} + \frac{\partial H}{\partial z} = 0$$

The state flux vector is given by

$$U = \left[\rho, \rho u, \rho v, \rho w, e^*, B_x, B_y, B_z \right]^T$$

with density ρ, velocities u, v and w, total energy per unit volume, including magnetic field energy, $e^* = e + \frac{1}{2\mu_e}B^2$, and B_x, B_y and B_z are the components of the magnetic field. $e = \rho(\varepsilon + \frac{1}{2}(u^2 + v^2 + w^2))$, ε represents the internal energy and $B^2 = B_x^2 + B_y^2 + B_z^2$. The flux vector F becomes

$$F = \begin{pmatrix} \rho u \\ \rho u^2 + p^* + \tau_{xx} - \frac{1}{\mu_e}B_x B_x \\ \rho v u + \tau_{xy} \quad - \frac{1}{\mu_e}B_x B_y \\ \rho w u + \tau_{xz} \quad - \frac{1}{\mu_e}B_x B_z \\ (e^* + p^* + \tau_{xx})u + \tau_{xy}v + \tau_{xz}w - k\frac{\partial T}{\partial x} \\ \quad + \frac{1}{\mu_e}\left(-(\vec{B}\cdot\vec{u})B_x + \beta_{xx}B_x + \beta_{xy}B_y + \beta_{xz}B_z \right) \\ \beta_{xx} \\ B_y u - B_x v + \beta_{xy} \\ B_z u - B_x w + \beta_{xz} \end{pmatrix}$$

with $p^* = p + \frac{1}{2\mu_e}B^2$ and magnetic stress given by $\beta_{ij} = -v_e\left(\frac{\partial B_j}{\partial x_i} - \frac{\partial B_i}{\partial x_j} \right)$. The magnetic field components shown above represent the total of the imposed and induced fields. The viscous stress tensor is given by $\tau_{ij} = -\mu\left(\frac{\partial u_i}{\partial x_j} + \frac{\partial u_j}{\partial x_i} \right) - \delta_{ij}\lambda\frac{\partial u_k}{\partial x_k}$, where δ_{ij} is the Kronecker delta. The other flux vectors G and H are similar.

The Jacobian of the inviscid part of the vector F (ie. with $\mu = \lambda = v_e = 0$) is given by $\frac{\partial F}{\partial U} = A = S^{-1}A'S$, with $S = \frac{\partial V}{\partial U}$, and $V = \left(\rho, u, v, w, B_x, B_y, B_z \right)^T$.

$$S = \begin{bmatrix} 1 & 0 & 0 & 0 & 0 & 0 & 0 & 0 \\ -\dfrac{u}{\rho} & \dfrac{1}{\rho} & 0 & 0 & 0 & 0 & 0 & 0 \\ -\dfrac{v}{\rho} & 0 & 0 & \dfrac{1}{\rho} & 0 & 0 & 0 & 0 \\ -\dfrac{w}{\rho} & 0 & 0 & 0 & \dfrac{1}{\rho} & 0 & 0 & 0 \\ \alpha\gamma^* & -u\gamma^* & -v\gamma^* & -w\gamma^* & \gamma^* & -B_x\gamma^* & -B_y\gamma^* & -B_z\gamma^* \\ 0 & 0 & 0 & 0 & 0 & 1 & 0 & 0 \\ 0 & 0 & 0 & 0 & 0 & 0 & 1 & 0 \\ 0 & 0 & 0 & 0 & 0 & 0 & 0 & 1 \end{bmatrix}$$

with $\alpha = \frac{1}{2}(u^2 + v^2 + w^2)$, $\gamma^* = \gamma - 1$ and γ represents the ratio of the specific heats of the gas.

$$A' = \begin{bmatrix} u & \rho & 0 & 0 & 0 & 0 & 0 & 0 \\ 0 & u & 0 & 0 & \dfrac{1}{\rho} & 0 & \dfrac{B_y}{\rho} & \dfrac{B_z}{\rho} \\ 0 & 0 & u & 0 & 0 & 0 & -\dfrac{B_x}{\rho} & 0 \\ 0 & 0 & 0 & u & 0 & 0 & 0 & -\dfrac{B_x}{\rho} \\ 0 & \gamma p & 0 & 0 & u & 0 & 0 & 0 \\ 0 & 0 & 0 & 0 & 0 & u & 0 & 0 \\ 0 & B_y & -B_x & 0 & 0 & 0 & u & 0 \\ 0 & B_z & 0 & -B_x & 0 & 0 & 0 & u \end{bmatrix}$$

The eigenvalues are

$$\lambda_{1,6} = u \,, \quad \lambda_{3,4} = u \pm \frac{B_x}{\sqrt{\rho}} \,, \quad \lambda_{2,5} = u \pm \sqrt{\frac{1}{2}\left(c^2 + \frac{B^2}{\rho} + \sqrt{\left(c^2 + \frac{B^2}{\rho} \right)^2 - 4c^2 \frac{B_x^2}{\rho}} \right)} \quad \text{and}$$

$$\lambda_{7,8} = u \pm \sqrt{\frac{1}{2}\left(c^2 + \frac{B^2}{\rho} - \sqrt{\left(c^2 + \frac{B^2}{\rho} \right)^2 - 4c^2 \frac{B_x^2}{\rho}} \right)}$$

The matrix A' and eigenvalues above were given by Powell along with the corresponding eigenvectors.

The flux vectors of the MFD equations are not *homogeneous of degree one* with respect to the state vector, but they can be trivially modified so that they become so. A method for their solution in conservation law form was presented

earlier[3-4]. The method uses upwind biased flux vectors directly instead of using the state vectors. This improves accuracy and allows for more flexibility in the eigenvector structure, which will be exploited later.

Modified Steger-Warming flux vector splitting is used to approximate the inviscid terms and central differences are used for the viscous terms. A block implicit algorithm, using modified approximate factorization with sub-iteration, was then used to solve the resulting set of finite volume difference equations. This numerical method also uses frame independent smoothing, and has the option of adapting the mesh to shock waves. The gas can be treated as a perfect gas or as a real gas in equilibrium.

2. Inclusion of Chemical Non-Equilibrium into the MFD Equations for Simulation of the Flow within MFD Generators and Accelerators for the Proposed Energy "Bypass Scram Jet Engine" Concept. (Items (4) and (5) in the Status of Effort Section above).

The following four reaction seeded air chemistry model of Park, Mehta and Bogdanoff, for temperatures to 4000K was used. The model employed here contains eight species. Species downstream of the combustor containing hydrogen were not included.

1) $O_2 + M \leftrightarrow O + O + M$

2) $N_2 + O \leftrightarrow NO + N$

3) $O + NO \leftrightarrow N + O_2$

4) $Cs + e^- \leftrightarrow Cs^+ + e^- + e^-$

The forward reaction rates, with parameters given in Tables 1-4, are of form.

$$k_f(T) = AT^n \exp(-T_r / T)$$

Table 1. $O_2 + M \leftrightarrow O + O + M$

M	A, m^8/(kg-mol.sec)	n	T_r, K
N2	5.09x10^12	-1.1	59,360
O2	5.09x10^12	-1.1	59,360
NO	1.27x10^13	-1.1	59,360
N	5.09x10^12	-1.1	59,360
O	5.09x10^12	-1.1	59,360
Cs	5.09x10^12	-1.1	59,360
Cs+	5.09x10^12	-1.1	59,360
e-	5.09x10^14	-1.1	59,360

Table 2. $N_2 + O \leftrightarrow NO + N$

A, m^8/(kg-mol.sec)	n	T_r, K
5.69e6	0.42	42,938

Table 3. $O + NO \leftrightarrow N + O_2$

A, m^8/(kg-mol.sec)	n	T_r, K
2.36e3	1.00	19,220

Table 4. $Cs + e^- \leftrightarrow Cs^+ + e^- + e^-$

A, m^8/(kg-mol.sec)	n	Tr, K
3.90e27	-3.78	45,180

The backward reaction rates, with parameters given in Table 5, are of form

$$k_b(T) = k_f(T)/k_{eq}(T) \quad , \text{ with } \quad k_{eq}(T) = \exp(A_1/z + A_2 + A_3 \ln(z) + A_4 z + A_5 z^2)$$

and $z = 10000/T$.

Table 5. Parameters k$_{eq}$, (MKS units)

	Reac. 1	Reac. 2	Reac. 3	Reac. 4
A$_1$	-0.9278	1.2441	2.3074	-4.1036
A$_2$	17.1414	0.7192	-2.9933	10.2278
A$_3$	0.2816	0.8606	1.2493	-3.4344
A$_4$	-6.0607	-3.9981	-1.8594	-4.2851
A$_5$	0.0027	0.0085	0.0087	-0.0097

The specie mole conversion rate equations become

$$R_1 = \sum_{m=1}^{8} \{k_{f1}[O_2][M_m] - k_{b1}[O][O][M_m]\}$$

$$R_2 = k_{f2}[N_2][O] - k_{b2}[NO][N]$$

$$R_3 = k_{f3}[O][NO] - k_{b3}[N][O_2]$$

$$R_4 = k_{f4}[Cs][e^-] - k_{b4}[Cs^+][e^-][e^-]$$

where the number of kilogram-moles/m^3 of species Z is defined by $[Z] = \rho_z / \omega_z$, species density ρ_z and molecular weight ω_z. The time dependent species mole equations are then

$$\frac{d[N_2]}{dt} = -R_2, \qquad \frac{d[N]}{dt} = +R_2 + R_3,$$

$$\frac{d[O_2]}{dt} = -R_1 + R_3, \qquad \frac{d[O]}{dt} = +2R_1 - R_2 - R_3,$$

$$\frac{d[NO]}{dt} = +R_2 - R_3, \qquad \frac{d[e^-]}{dt} = +R_4,$$

$$\frac{d[Cs]}{dt} = -R_4, \qquad \frac{d[Cs^+]}{dt} = +R_4$$

The heats of formation, energy taken from the gas internal energy to form species, are given in Table 6., in Joules/kilogram, along with species molecular weights and the initial concentrations, species density divided by total gas density, $c_z = \rho_z / \rho$.

Table 6. Physical Properties of Gas

	ω	Initial c$_z$	Heat of Form.
N2	28.01	0.76290	0.0
O2	32.00	0.23695	0.0
NO	30.07	0.0	2.996123x10^6
N	14.01	0.0	3.362161x10^7

O	16.00	0.0	1.543119x10^7
Cs	132.9	0.00015	0.0
Cs+	132.9	0.0	2.899905x10^6
e-	54.2*	0.0	0.0

* indicates x10^-5

Also, equations for species convection and diffusion need to be solved.

$$\frac{\partial c_z}{\partial t} = -u_i \frac{\partial c_z}{\partial x_i} + \frac{1}{\rho} \cdot \frac{\partial \mu_z \frac{\partial c_z}{\partial x_i}}{\partial x_i}, \qquad z = 1,8$$

The species mole equations are solved implicitly by sub-iteration in time. We can write them in vector form as $\frac{dS}{dt} = R(S)$. S is a vector containing the 8 species mole elements and $R(S)$ contains the 8 right hand sides of the above equations. The sub-iteration procedure converges $R(S^{n+1}) - \frac{S^{n+1} - S^n}{\Delta t}$ to zero as follows.

$$\{I + \Delta\tau\hat{A}\}\left(S^{(m+1)} - S^{(m)}\right) = \Delta\tau\left(R(S^{(m)}) - \frac{S^{(m)} - S^n}{\Delta t}\right)$$ with $S^{(0)} = S^n$ and $S^{(m)} \to S^{n+1}$ as $m \to \infty$, $\Delta\tau$ is

chosen appropriately small and $\hat{A} = \frac{\partial R}{\partial S}$ is the Jacobian of R with respect to S. The sub-iteration procedure is stopped when the maximum change in concentration of each species is less than 10^6. The species convection-diffusion equations are solved using upwind implicit finite volume approximations.

2-D simulations of the flow of air within an MHD generator were made with seeded cesium. The generator was a square duct, 2.721m long, of height/width 64.85cm at the entrance and of height/width 85.14m at the exit. The magnetic field across the channel was 12.74 Tesla and the transverse voltage gradient was -29,400 V/m at the entrance and -18,290 V/m at the exit. The numerical simulation varied this voltage linearly from entrance to exit. At the entrance the pressure p=1,038x10^6 Pa, temperature T=3371°K, and the Mach number equaled 2.418. The electrical conductivity was enhanced by the seeding with liquid cesium. The Park program for calculating conductivity had difficulties near the wall, which was held at a fixed wall temperature of T=300°K, and had to numerically limited within the boundary layer to levels predicted by the Park program at the edge of the boundary layer. This difficulty was later removed, as will be discussed later. The results for finite rate chemistry and conductivity calculated from the Park program are shown in Figs.4-6.
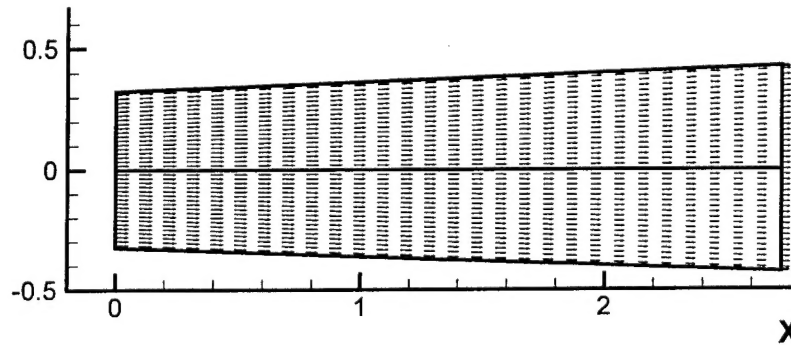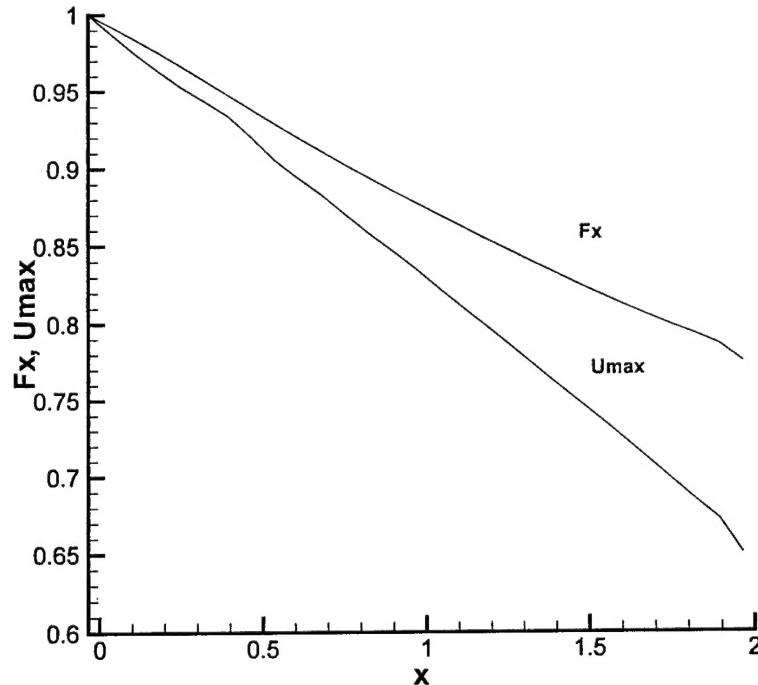

Figure 1. Velocity profiles within MHD generator, reacting seeded air chemistry.

The⊠supersonic⊠velocity⊠profiles⊠within⊠the⊠generator,⊠shown⊠along⊠the⊠center⊠
plane⊠in⊠Fig.1,⊠decelerate⊠significantly⊠in⊠the⊠diverging⊠duct⊠while⊠generating⊠
electric⊠power.⊠

Figure 2. Normalized force and velocity in axial direction within MHD generator section, reacting seeded air chemistry

Normalized⊠axial⊠force⊠ F_x ⊠and⊠maximum⊠velocity⊠as⊠a⊠function⊠of⊠ x ⊠are⊠shown⊠in⊠

Fig.2.⊠Note⊠that⊠within⊠the⊠generator⊠both⊠ F_x ⊠and⊠ u_{max} ⊠decrease⊠significantly.⊠

3. An Alternative Formulation of the Equations of Magneto-fluid-Dynamics - The Reduced MFD Equations in Conservation Form (Item (6) in the Status of Effort Section above).

An alternate formulation of the governing equations of magneto-fluid-dynamics has been devised. This formulation is mathematically equivalent to the original set of equations governing magneto-fluid-dynamics given above, including magnetic self induction, and retains the conservation law form of the equations and their eigenvalues. This new set has advantages over the original set when solved numerically for flows within strong imposed magnetic fields.

The formulation treats the imposed and induced fields separately. Though ever present, the imposed field remains in the background as the finite volume difference equations focus on the induced field. The imposed field can not be eliminated entirely from the difference equations because of non-linearity, but no squared imposed magnetic field terms appear. This is important for flows within strong imposed magnetic fields, because the magnetic pressure, proportional to the square of the imposed magnetic field strength, can be several orders of magnitude larger than the aerodynamic pressure or the induced magnetic field pressure. Numerical errors in the very large magnetic stress

difference terms of the imposed field could be of significance when combined with the relatively smaller fluid stress terms.

Before the introduction of this alternative formulation, there were two choices for including the effects of a magnetic field upon an ionized flow: (1) the complete equations of magneto-fluid-dynamics, including magnetic induction and (2) the inclusion of the "j cross B" force and Joule heating effects in the Navier-Stokes equations as additional source terms. The first choice is a set of eight equations consisting of the Navier-Stokes equations, with added magnetic stress tensor, plus the Maxwell inductions equations and is presented in Sec.1. above. The second choice, a set of five equations, called the "Low Magnetic Reynolds Number Approximation", assumes that the induced magnetic field is negligible. It is far more efficient and has far fewer numerical difficulties associated with inclusion of magnetic effects than the first choice. There is, however, some uncertainty in when the low magnetic Reynolds number is valid, even for aerodynamic flows of current interest. The now available third choice presented below can be used to investigate this question.

The total magnetic field consists of the imposed magnetic field, $\vec{B}_0$, and the induced magnetic field, $\vec{B}_i$, and $\vec{B}_t = \vec{B}_0 + \vec{B}_i$, where the subscripts t, 0 and i now and below indicate *total, imposed and induced* magnetic components. For cases for which the induced field is much less than the imposed field, but not negligibly small, we can benefit by rewriting the Lorentz force as $\vec{L}_f = \dfrac{1}{\mu_e}(\vec{\nabla} \times \vec{B}_i) \times \vec{B}_t$,

because the imposed magnetic field is generated by currents external to the flow field, for which $\vec{\nabla} \times \vec{B}_0 = 0$. The approach taken here is similar to the simplification in electromagnetic scattering where only the disturbed field is calculated, with nothing lost by the separation of the two fields.

We can also write the Lorentz force as $\vec{L}_f = \dfrac{1}{\mu_e}(\vec{\nabla} \times \vec{B}_t) \times \vec{B}_t - \dfrac{1}{\mu_e}(\vec{\nabla} \times \vec{B}_0) \times \vec{B}_0$, and through some algebraic manipulation, the Lorentz force can be brought into the flux derivative terms of the momentum equation, in conservation law form as before. The state vector becomes $U = \left[\rho, \rho u, \rho v, \rho w, e^*, B_{i_x}, B_{i_y}, B_{i_z} \right]^T$ and the new flux vector F becomes

$$
F = \begin{pmatrix}
\rho u \\
\rho u^2 + p^* + \tau_{xx} - \frac{1}{\mu_e}B_{i_x}B_{t_x} w - \frac{1}{\mu_e}\{B_{i_x}B_{0_x}\} \\
\rho v u + \tau_{xy} \qquad - \frac{1}{\mu_e}B_{i_y}B_{t_x} \quad - \frac{1}{\mu_e}\{B_{i_x}B_{0_y}\} \\
\rho w u + \tau_{xz} \qquad - \frac{1}{\mu_e}B_{i_z}B_t \quad - \frac{1}{\mu_e}\{B_{i_x}B_{0_z}\} \\
(e^* + p^* + \tau_{xx})u + \tau_{xy}v + \tau_{xz}w - k\frac{\partial T}{\partial x} \\
\qquad + \frac{1}{\mu_e}\left(-(\vec{B}_i \cdot \vec{u})B_{t_x} + \beta_{xx}B_{i_x} + \beta_{xy}B_{i_y} + \beta_{xz}B_{i_z}\right) \\
\beta_{xx} \\
B_{t_y}u - B_{t_x}v + \beta_{xy} \\
B_{t_z}u - B_{t_x}w + \beta_{xz}
\end{pmatrix}
$$

with $p^* = p + \frac{1}{2\mu_e}B_t^2 + \frac{1}{\mu_e}\vec{B}_i \cdot \vec{B}_t$ and the magnetic

stress given by $\beta_{ij} = -v_e\left(\dfrac{\partial B_{i_j}}{\partial x_i} - \dfrac{\partial B_{i_i}}{\partial x_j}\right)$

By replacing the magnetic pressure, $\frac{1}{2\mu_e}B_t^2$, by the smaller $\frac{1}{2\mu_e}B_i^2 + \frac{1}{\mu_e}\vec{B_i}\cdot\vec{B_t}$, the magnetic and static pressures are closer in magnitude for strong imposed magnetic fields. Favorable reductions also take place in the induction equations because the magnetic diffusion terms β_{ij} are just components of the curl of the induced magnetic field times v_e. Again the imposed field, produced by currents outside the flow field, is curl free. Hence, $v_e\vec{\nabla}\times\vec{B_t} = v_e\vec{\nabla}\times\vec{B_i}$. Here also the production and diffusion terms are more equally balanced. Finally, the terms in the curly brackets in the momentum equations above vanish if the imposed field is constant in space because of the divergence free nature of both the imposed and induced fields.

One may assume that the structural changes to the equations, just presented, from the separation of the induced and imposed fields, would have profound changes to the original eigenvalue-eigenvector structure of the equations. Fortunately, the eigenvalues remain the same as shown below.

$$\lambda_{1,6} = u, \quad \lambda_{3,4} = u \pm \frac{B_{t_x}}{\sqrt{\rho}}, \lambda_{2,5} = u \pm \sqrt{\frac{1}{2}\left(c^2 + \frac{B_t^2}{\rho} + \sqrt{\left(c^2 + \frac{B_t^2}{\rho}\right)^2 - 4c^2\frac{B_{t_x}^2}{\rho}}\right)} \text{ and}$$

$$\lambda_{7,8} = u \pm \sqrt{\frac{1}{2}\left(c^2 + \frac{B_t^2}{\rho} - \sqrt{\left(c^2 + \frac{B_t^2}{\rho}\right)^2 - 4c^2\frac{B_{t_x}^2}{\rho}}\right)}$$

The eigenvectors are changed, however, but the original set can still be used in the solution procedure as is to solve the alternative RMFD (Reduced Magneto-Fluid Dynamics) equations just presented, because of the conservation form of the flux vector splitting used.

The term *Reduced* is used here to reflect the notion that the magnitude of the magnetic terms are reduced by removing as often as possible the imposed magnetic field from them, although the number of terms is actually increased. The RMFD equations are mathematically and physically equivalent to the original MFD equations.

4. The Navier-Stokes Equations Plus a Source Term for Magnetic Field Effects - The Low Magnetic Reynolds Number Approximation

An ionized flow within an imposed magnetic field can self induce, thus changing the magnitude of the total magnetic field. The relative magnitude of the induced component depends upon the Magnetic Reynolds number, defined by $R_m = u_0 l_0 \sigma_e \mu_e$, where u_0 and l_0 are reference flow speed and length, σ_e is the gas conductivity and , μ_e is the magnetic permeability. The magnetic diffusion coefficient is given by $v_e = \dfrac{1}{\sigma_e\mu_e}$. For most aerodynamic flows the gas conductivity is very small and, consequently, v_e is very large and the magnetic Reynolds number is less than one. In such cases, any self induced magnetic field supposedly rapidly diffuses away, leaving only the imposed magnetic field. This leads to a great simplification in calculating the electro-magnetic effects upon an ionized flow. This approach, *The Low Magnetic Reynolds Approximation approach,* only needs to add a source term to the flow equations given above to include the electro-magnetic field effects.

Ionized flow in the presence of a magnetic or electric field generates a current, according to Ohm's law, $\vec{j} = \sigma_e(\vec{E} + \vec{u} \times \vec{B})$, where $\vec{j}$ is the current density, $\vec{E}$ is the electric field potential, $\vec{u}$ is the flow velocity and $\vec{B}$ is the magnetic field. The electric current itself interacts with the magnetic field to create a Lorentz force, $\vec{L}_f = \vec{j} \times \vec{B}$, that acts on the flow in addition to pressure, p, and viscous stress.

In addition to the Lorentz force added to the momentum equations, Joule heating, caused by the flow of electric current through the fluid, plus magnetic force work terms need to be added to the energy equation. The equations become

$$\frac{\partial U}{\partial t} + \frac{\partial F}{\partial x} + \frac{\partial G}{\partial y} + \frac{\partial H}{\partial z} = S$$

The state, flux vectors and the source vector are given by $U = [\rho, \rho u, \rho v, \rho w, e]^T$

$$F = \begin{pmatrix} \rho u \\ \rho u^2 + p + \tau_{xx} \\ \rho vu + \tau_{xy} \\ \rho wu + \tau_{xz} \\ (e + p + \tau_{xx})u + \tau_{xy}v + \tau_{xz}w - k\frac{\partial T}{\partial x} \end{pmatrix}, \text{etc, } \boxtimes\boxtimes\text{and}\boxtimes\boxtimes\boxtimes\ S = \begin{pmatrix} 0 \\ (\vec{j} \times \vec{B})_x \\ (\vec{j} \times \vec{B})_y \\ (\vec{j} \times \vec{B})_z \\ (\vec{j} \times \vec{B}) \cdot \vec{u} + \frac{1}{\sigma_e}\vec{j} \cdot \vec{j} \end{pmatrix}$$

This equation set is sufficient to describe ionized flow within an electro-magnetic field, as long as the fields are specified. It is not much more difficult to solve than the underlying Navier-Stokes flow equations themselves. However, if the magnetic field varies in time by self induction and the induced magnetic components are relatively significant in magnitude then the equations for magnetic induction also need to be solved. This larger set, shown earlier in Sec. 1., is much more difficult to solve and should not be attempted if it can be avoided.

5. Comparison of the Full MFD Equations, the Reduced MFD Equations ans the Low Reynolds Number Equations

The figure below shows the velocity field within the accelerator region of a proposed energy bypass scram engine, locate just downstream of the combustor.
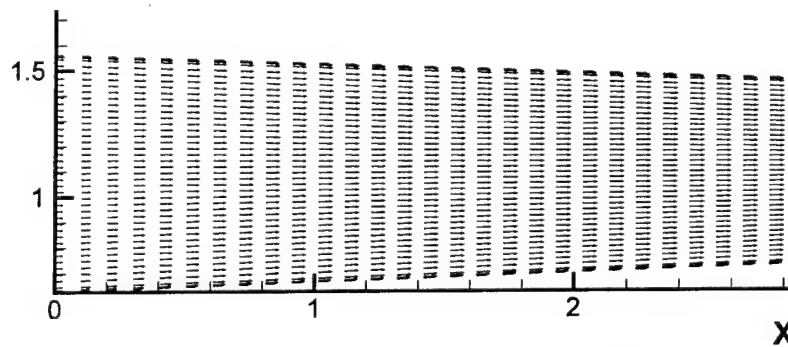
Figure 3. Velocity profiles within an MHD accelerator, reduced MHD simulation
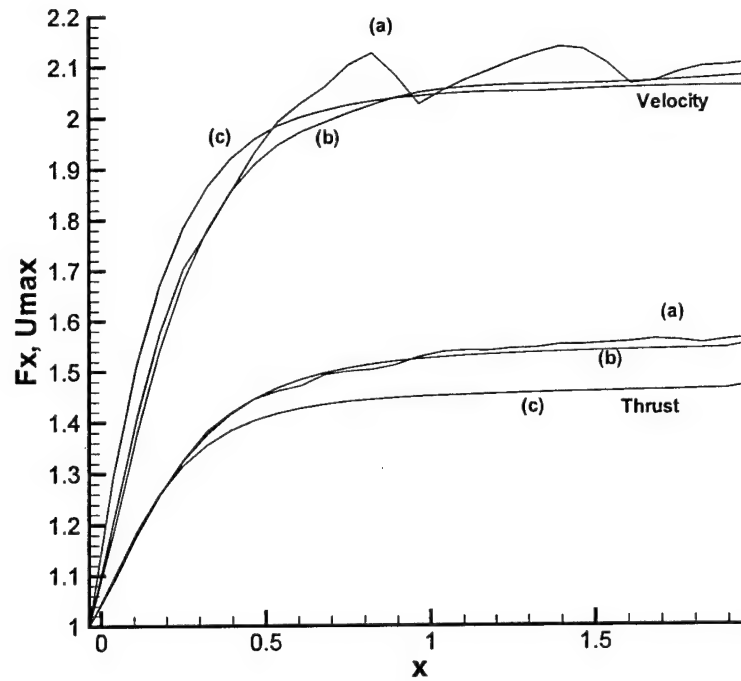
Figure 4. Normalized Force and velocity in the axial direction within an MHD accelerator section, (a) Full MFD, (b) Reduced MFD and (c) Low Magnetic Reynolds Number

The supersonic velocity profiles within the accelerator are shown in Fig.3 to accelerate significantly in the converging duct. These results were obtained from the Reduced MFD set of equations. This set of equations is mathematically equivalent to the full set of MFD equations, but the imposed and induced magnetic fields are separated. The imposed field is constant and can often be extracted from derivatives in the governing equations. This is numerically helpful when the imposed field is much larger than the induced magnetic field and consequently the imposed magnetic pressure, proportional to the magnitude of the imposed field squared, is orders of magnitude greater than the aerodynamic pressure. The reduced set of equations, called Reduced MFD herein, is still in conservation form and has the same eigenvalue structure, but is numerically better posed. The Low Magnetic Reynolds Number Approximation neglects the induced terms entirely. The Reduced MFD formulation was not foreseen in the original proposed research, but developed subsequently after strong magnetic fields were introduced into the study to simulate flows of Air Force interest.

Normalized axial force F_x and maximum velocity u_{max} are shown within the accelerator in Fig.4. All three simulations, (a) the full MFD, (b) the reduced MFD and (c) the Low Magnetic Reynolds Number Approximations are shown. The induced magnetic field for both the Reduced and full MFD approaches was approximately 1% of the imposed field strength. Note for each case that both F_x and u_{max} increase significantly at first then level off as the flow traverses the duct. The full MFD results for velocity show unexpected spatial variations, perhaps caused by the numerical difficulties discussed earlier. Also, the Low Magnetic Reynolds Number Approximation is not in agreement for calculated thrust with the other results that include magnetic induction. It is about 20% lower. This finding can be very significant. If the Low Reynolds Number Approach is found to be physically incorrect for flows at magnetic Reynolds Numbers less than one, as in the case here, their use to simulate flows within magnetic and electric fields will have little confidence. The small 1% change in magnetic field caused

by induction results in a magnetic pressure of the order of the gas pressure itself and could explain this effect. Further study, required to determine the significance and validity of these results is pursued in the next section.

6. Analysis of the Physics of Upstream Influence Caused by Magnetic Diffusion and the Eigenvalue Properties of the MFD Equations in Comparison with the simpler "Low Magnetic Reynolds Number" Approach for Flows within MFD Generators and Accelerators. (Item (7) in the Status of Effort Section above).

6.1 Simple test geometry problem

These figures demonstrate that the two mathematical formulations describe different physics. On the Shown below are the results from the three numerical simulations for flow within an MFD accelerator with a simplified geometry. The 2D channel consists of a rectangular volume 3m. long and 1m. high. The wall temperatures were held fixed at 300°K. The imposed magnetic field was $B_y = 11$ Tesla and the electric field was $E_z = -30,000$ V/m. The equilibrium flow entering the channel was at Mach 1.166 with total pressure, 8×10^5 N/m^2 and total temperature 7500°K. The electrical conductivity was held uniform within the accelerator at $\sigma = 36.0/(\Omega m)$ and the magnetic Reynolds number $R_m = u_0 l_0 \sigma_e \mu_e = 0.1847$.

Top Electrode

$$M_o = u_o / c_o = 1.166$$

Flow

$$M_{mag} = u_o / c_f = 0.148$$

Bottom Electrode
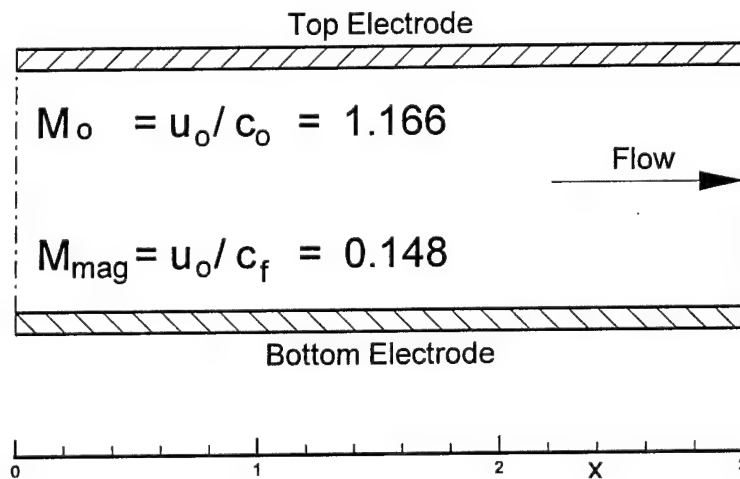
The acceleration of the velocity vectors is shown in Fig.5. These results were obtained from the Reduced MFD set of equations. Normalized axial force, $F_x(x) = \int_{S(x)} (\rho u^2 + p)\ ds$, integrated across the channel, and maximum velocity u_{max} are shown within the accelerator in Fig.6 for all three simulations. The maximum induced magnetic field was less than 2% of the imposed field strength. Note for each case that both F_x and u_{max} increase significantly at first then level off as the flow traverses the duct. The Full MFD results for velocity show some unexpected spatial variations, perhaps caused by the numerical difficulties discussed earlier. Also, the Low R_m MFD result is not in agreement for calculated thrust with the other results that include magnetic induction. It is about 8% lower. The small 2% change in magnetic field caused by induction results in a magnetic pressure of the order of the gas pressure itself and was first thought to be responsible for this effect
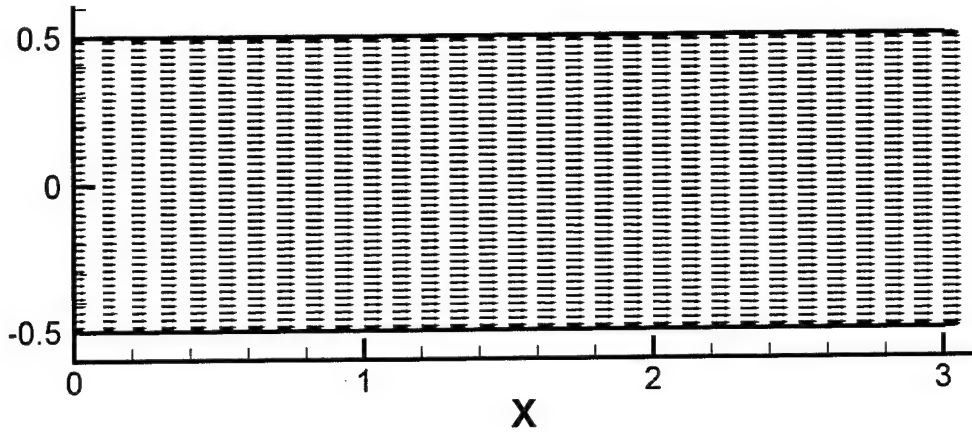
Figure 5. Velocity profiles within an MHD accelerator, Reduced MHD simulation
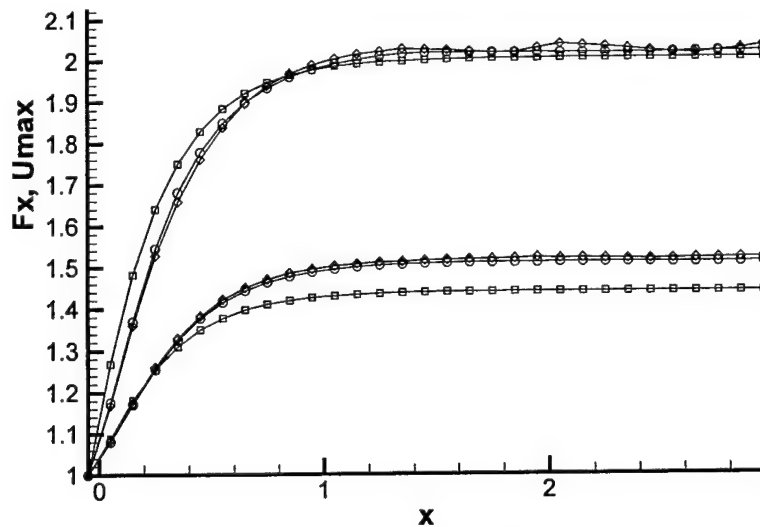
Figure 6. Normalized Force (bottom) and velocity (top) in the axial direction within an MHD accelerator section, (a) Full MFD - diamonds, (b) Reduced MFD - circles and (c) Low R_m MFD – squares

6.2 Possible Causes for Differences

Consider the following explanations for the differences in computed results:

(1) Errors in the numerical procedures caused the difference in results.
(2) The small induced magnetic fields are significant enough to change the magnetic stress, work and heating within the flow field.
(3) The eigenvalue-vector structure of the equations is different enough to significantly alter domains of dependence and influence within the flow field.

6.2.1 Numerical error in solving the equations

Unfortunately, numerical error is always present despite the most exhausting steps to prevent it and it should be the first consideration. The test channel accelerator problem was made as simple as possible to reduce potential error. The geometry is Cartesian-like, the magnitudes of the magnetic field, electric field and electrical conductivity were constants, the flow was supersonic, except within the boundary layer and the solutions were steady state. A single program was written to solve each set of equations.

Hopefully, only the equations changed and not the solution procedure for solving them. The Low R_m MFD set of equations was always the easiest to solve and the fastest to converge. The Full MFD equations were the most difficult to solve, but they should give the right answer if solved correctly and should be able to be used to tell when the simpler sets suffice. However, it will probably be quite awhile before we can solve them with confidence for all engineering flows of interest to hypersonic vehicle design. Much more experimentation will be required for validation of numerical simulations of MFD flows.
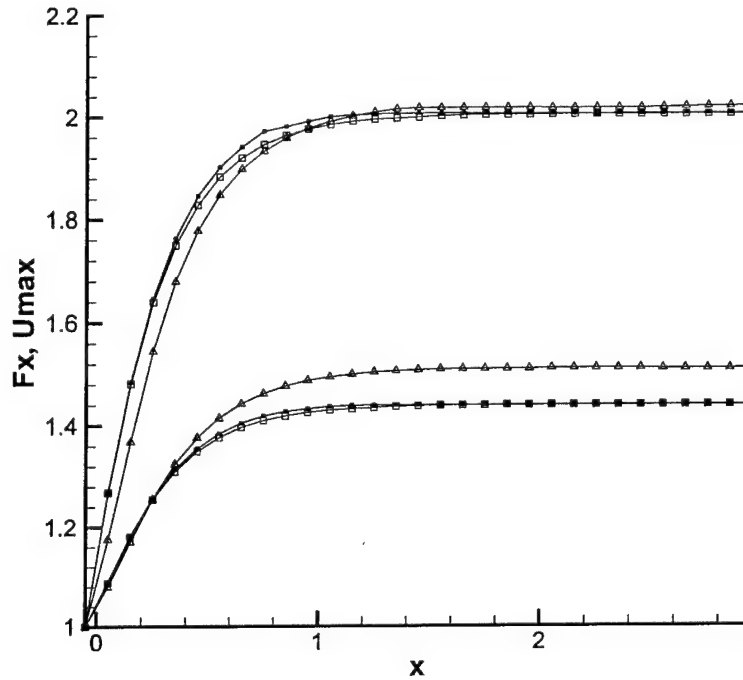
Figure 7. Normalized Force and velocity (a) Reduced MFD – circles, (b) original Low R_m MFD, – squares and (c) Low R_m MFD, using the total magnetic field from the above Reduced MFD solution – small squares

6.2.2 Induced magnetic field may significantly change magnetic stress
To test out this hypothesis an additional calculation was made. The induced magnetic field from the solution of the Reduced MFD set of equations was added to the imposed field and used as an initial condition for the Low R_m MFD set of equations. Therefore, both sets of equations had the same magnetic fields at steady state. The results are shown in Fig.7. Although there are small differences between the two Low R_m MFD solutions they end up with the same thrust and velocity at the exit. Therefore the small difference in magnetic induction is not the cause of the difference in the thrust observed earlier.

6.2.3 The different eigenvalue-vector structure
The eigenvalue-vector structure of the equations is different. The Low R_m MFD set of five equations has the same eigenvalues and eigenvectors of the underlying Euler or Navier-Stokes equations. These eigenvalues for the flux in the x-direction are $\lambda_{1,3,4} = u$ and $\lambda_{2,5} = u \pm c$, where u is the velocity in the x-direction and c is the speed of sound. These eigenvalues determine the domains of mathematical and hence assumed physical domains of dependence and influence. For the MFD channel accelerator case the flow is supersonic except within a very thin boundary layer at the walls. Therefore all the

eigenvalues are positive and permit no upstream influence. The Navier-Stokes equations also permit diffusion because of viscosity. But outside the boundary layer viscous diffusion is insignificant for the flow Reynolds number of the test problem.

The eigenvalues for the flux in the x-direction for the Full or Reduced MFD eight equation set are

$$\lambda_{1,6} = u, \quad \lambda_{3,4} = u \pm \frac{B_x}{\sqrt{\rho}}, \quad \lambda_{2,5} = u \pm \sqrt{\frac{1}{2}\left(c^2 + \frac{B^2}{\rho} + \sqrt{\left(c^2 + \frac{B^2}{\rho}\right)^2 - 4c^2\frac{B_x^2}{\rho}}\right)} \quad \text{and}$$

$$\lambda_{7,8} = u \pm \sqrt{\frac{1}{2}\left(c^2 + \frac{B^2}{\rho} - \sqrt{\left(c^2 + \frac{B^2}{\rho}\right)^2 - 4c^2\frac{B_x^2}{\rho}}\right)}$$

where B^2 is the square of the magnetic field, B_x is the x-component and ρ is the density. $\lambda_{3,4}$ are the Alfven wave speeds and $\lambda_{2,5}$ and $\lambda_{7,8}$ are called the fast and slow magnetic wave speeds. If the magnetic field is zero in magnitude, $\lambda_{7,8}$ vanish and both sets of eigenvalues are equal. In addition to viscous diffusion, magnetic diffusion, which can be orders of magnitude larger, can spread information omni-directionally. Even though the flow is conventionally said to be supersonic in the x-direction for the test case problem, all the eigenvalues are not positive and information can easily travel upstream. The magnetic Mach number $M_{mag} = u/c_f = 0.148$ at the entrance, where c_f is the fast magnetic wave speed and is given above by the large square root term appearing in the equation for $\lambda_{2,5}$ above.

The governing equations are meant to match the assumed physics and moreover vice versa. Here the physics corresponding to the two descriptions, Full MFD and Low R_m MFD are definitely different. Is this difference responsible for observed differences in the flow simulations?
The answer is yes, which we can demonstrate with a little analysis. First, the Lorentz force is given below.

6.3 The different eigenvalue-vector structure
The eigenvalue-vector structure of the equations is different. The Low R_m MFD set of five equations

$$\vec{L}_f = \frac{1}{\mu_e}(\vec{\nabla}\times\vec{B})\times\vec{B} = \sigma_e(\vec{E} + \vec{u}\times\vec{B})\times\vec{B} .$$ The Low R_m MFD equations evaluate the Lorentz force term

by the expression to the right of the last equal sign above and the Full MFD equations by that to the right of the first equal sign above. For the two dimensional test flow problem the curl of the magnetic field has only a z-direction component.

$$D_z = (\vec{\nabla}\times\vec{B}_i)_z = \frac{\partial B_y}{\partial x} - \frac{\partial B_x}{\partial y}$$

Second, we can express the induction equations as

$$\frac{\partial B_x}{\partial t} = -\frac{\partial(vB_x - uB_y + v_e D_z)}{\partial y} = -\frac{\partial E_z}{\partial y}$$

$$\frac{\partial B_y}{\partial t} = +\frac{\partial(vB_x - uB_y + v_e D_z)}{\partial x} = +\frac{\partial E_z}{\partial x}$$

and finally from them form a Poisson equation for D_z as follows.

$$\frac{\partial D_z}{\partial t} = \frac{\partial^2 E_z}{\partial x^2} + \frac{\partial^2 E_z}{\partial y^2}$$

We can solve this equation in an extended domain of the channel flow problem to illustrate the powerful upstream and downstream influence of the induction equations. Earlier the domain enclosed only the flow between the two electrodes extending from x=0 to x=3m. The extended domain covers the flow ahead and downstream of the electrodes by 1m. each.

Figs.8 and 9 show the solutions for E_z and D_z from the Poisson equation on this domain. They represent solutions to the Full and Reduced MFD equations.
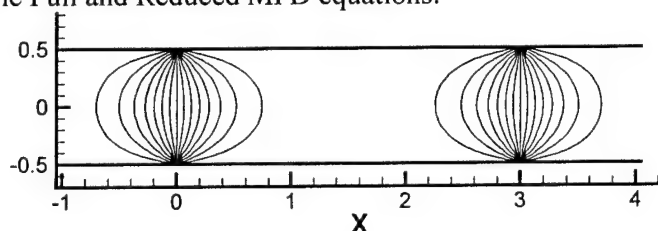
Figure 8. Contours of E_z on extended domain
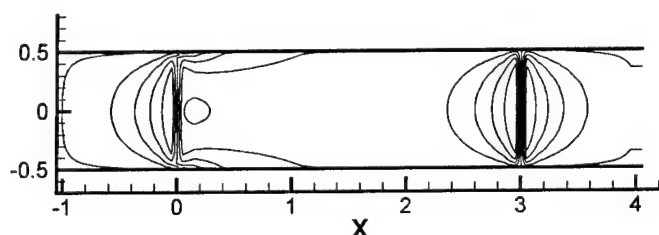
Figure 9. Contours of D_z on extended domain

Note the upstream propagation of E_z for the Full MFD solution in Fig.8 and the strong gradients and upstream propagation in D_z shown in Fig.9, both of which could not be simulated using the Low R_m MFD approach.

6.4 Conclusion for test problem results
These figures demonstrate that the two mathematical formulations describe different physics. On the original domain the Low R_m MFD description behaved exactly as a conventional supersonic flow with no apparent upstream influence. On the other hand, the Full MFD approach, through the fast magnetic wave speed and high magnetic diffusion, did allow upstream influence even at the upstream boundary, from which the flux split procedure accepted only information carried along characteristics needed for the downstream solution. The differences shown earlier in thrust prediction resulted not from different velocity distributions but from different mass flow rates entering the channel caused by upstream influence.

However, there is considerable doubt that placing this boundary at the start of the electrodes for the Full MFD set of equations, as shown above for the simple test case geometry, allowed proper upstream influence in view of the rapid gradients shown above at x=0m. in Fig.9. These calculations need to be repeated with the upstream boundary located sufficiently far ahead of the electrodes, as shown in the next subsection.

6.5 Extended accelerator geometry test problem
The channel was extended 1.5 meters both ahead and aft of the imposed electrode and magnetic field section, thereby placing the boundaries at sections of the flow that are supersonic with respect to all wave speeds of sound. The equations of the Full MFD Approach will induce a magnetic field beyond the electrode-imposed magnetic field location, but it should not be strong enough to produce magnetic
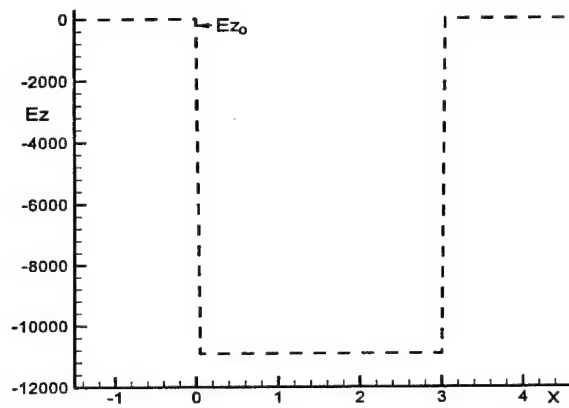
waves capable of reaching the upstream boundary. The flow within the extended channel will be simulated again using both approaches and then analyzed and discussed.
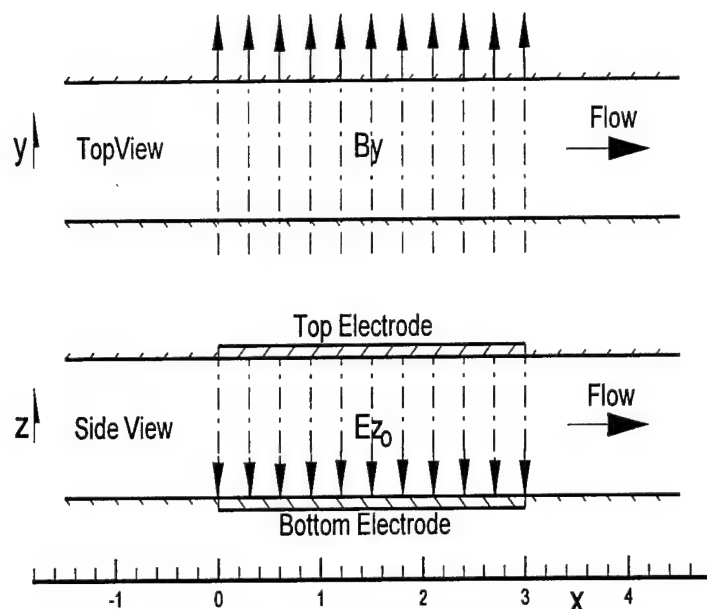
Figure 10. Sketch of Extended MFD Accelerator
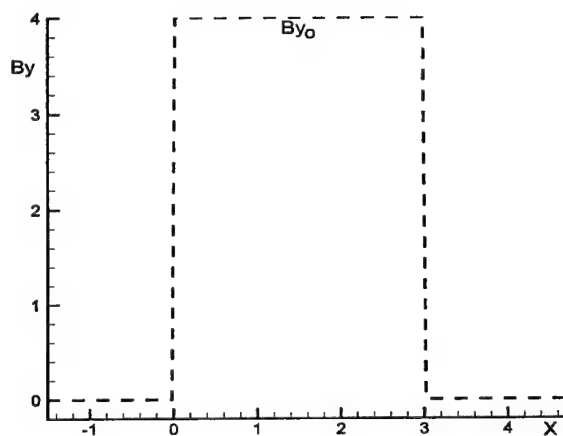
Figure 11. Imposed Magnetic Field

Figure 12. Imposed Electric Field

The extended MFD accelerator geometry is shown in Fig.10 and the imposed electric and magnetic fields in Figs.11 and 12. The discontinuities in these fields present simulation difficulties. For example, the magnetic pressure suddenly jumps to a value several times that of the fluid static pressure at $x=0$ and then back down again at $x=3m$. The equations describing this flow and a needed reformulation for them, designed to overcome the simulation difficulty, are given in the following section.

The imposed magnetic field was $B_{yo} = 4$ Tesla and the electric field was $E_{zo} = -10,909$ V/m., creating a load factor of 2.004. The wall temperatures were held fixed at 300°K and the initial flow speed was 1361m/sec The equilibrium flow entering the channel was at Mach 1.166, with pressure 1.251×10^6 N/m² and temperature 3,583°K. The electrical conductivity was held uniform within the accelerator at $\sigma = 36.0/(\Omega m)$ and the magnetic Reynolds number $R_m = u_0 l_0 \sigma_e \mu_e = 0.1847$.
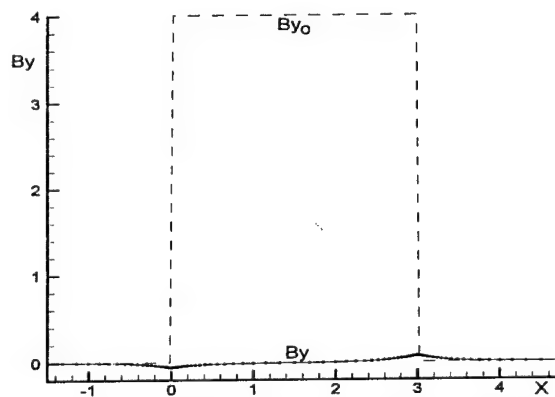
Figure 13. Solution for $\mathbf{B_y}$ along centerline.
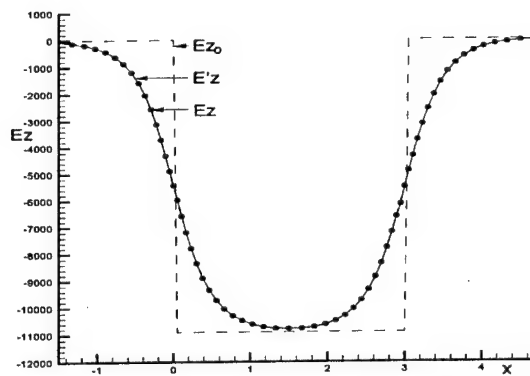
Figure 14. Solutions for $\mathbf{E_z}$ along centerline

.The solutions for B_y and E_z are shown in Figs. 13 and 14, along the channel centerline. Note the relatively small induced magnetic field. The solution of the "Equation for E_z" of Subsec.6.3 above is denoted by E'_z. It was solved independently of the MFD equations of Subsec.6.3. The solution of the MFD equations is denoted by E_z and the solid symbols. The two solutions are in excellent agreement, which is a validation of the MFD simulation.
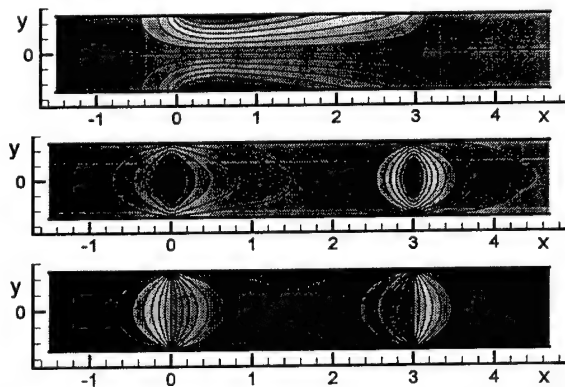
Figure 15. $\mathbf{B_x}$ (top), $\mathbf{B_y}$ (middle) and $\mathbf{E_z}$ fields.
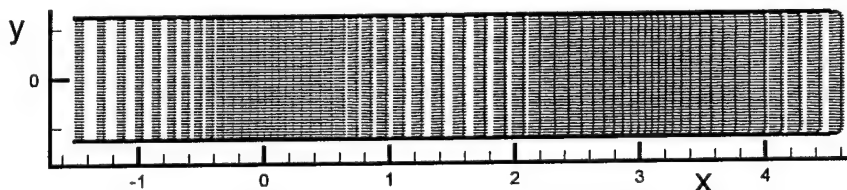
Figure 16. Velocity Field
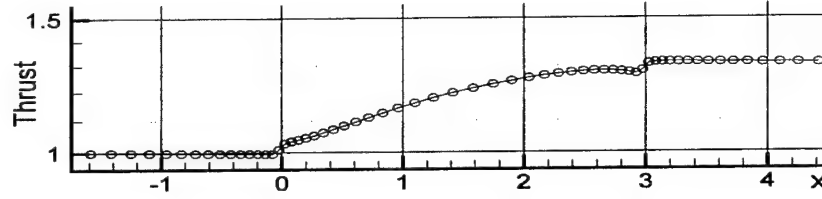
Figure 17. Thrust, $F_x(x) = \int\limits_{S(x)} (\rho u^2 + p)\ ds$

6.5.1 A Serious Problem Concerning the Results Given Above

The solution to the MFD Equations was fully converged. That is, it satisfies the governing equations relaxed to steady state and it also is in excellent agreement with the results for the "Equation for E_z" of Subsec.6.3 above. But, perhaps the reader noticed that it does not satisfy the constraint that the induced field be divergence free.

6.6 Divergence of B Control

6.6.1 Artificial "Compressibility" Approach

For incompressible flow, artificial compressibility is often used to steer the velocity field toward being divergence free. An artificial compressibility term proportional to the divergence of the velocity field is added to the pressure, $p \leftarrow p + \beta(\vec{\nabla} \cdot \vec{u})$. Similarly, to control divergence of the magnetic field, we add the term $\nu_e(\vec{\nabla} \cdot \vec{B})$ to the induction equations.

New 2-D Induction Equations -

$$\frac{\partial B_x}{\partial t} = -\frac{\partial \nu_e(\vec{\nabla} \cdot \vec{B})}{\partial x} - \frac{\partial(vB_x - uB_y + v_eD_z)}{\partial y}$$

$$\frac{\partial B_y}{\partial t} = +\frac{\partial(vB_x - uB_y + v_eD_z)}{\partial x} - \frac{\partial \nu_e(\vec{\nabla} \cdot \vec{B})}{\partial y}$$

The results given earlier did use the above equation, but it was not sufficient to prevent $\vec{\nabla} \cdot \vec{B}$ from becoming too large. Though it did, perhaps, prevent runaway growth.

6.6.2 Poisson Equation Approach

Full Poisson Equation Approach

First a Poisson Equation for a scalar function ϕ is solved $\frac{\partial^2 \phi}{\partial x^2} + \frac{\partial^2 \phi}{\partial y^2} = -\vec{\nabla} \cdot \vec{B}$. Then the magnetic field components are modified to be divergence free, as follows.

$$B_x \leftarrow B_x + \frac{\partial \phi}{\partial x} \quad and \quad B_y \leftarrow B_y + \frac{\partial \phi}{\partial y}$$

<u>Partial Poisson Equation Approach</u>

A 1-D Poisson Equation for ϕ is solved at each flow field point. $\dfrac{\partial^2\phi}{\partial y^2} = -\vec{\nabla}\cdot\vec{B}$. The x magnetic field component is kept as is, but the y component is then modified, $B_y \leftarrow B_y + \dfrac{\partial\phi}{\partial y}$, to maintain a divergence free magnetic field.
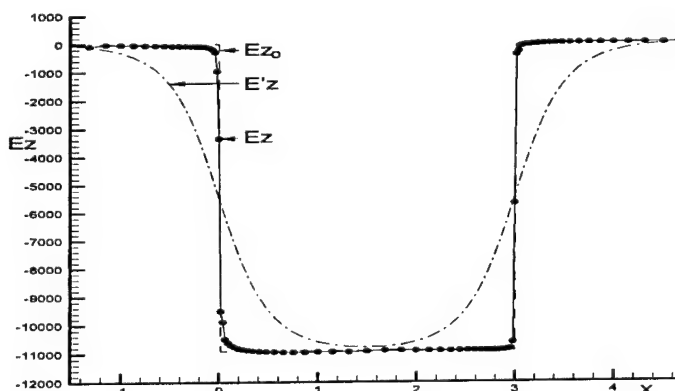
6.7 New Computational Results for Extended MFD Accelerator
The flow field was recalculated, using the Partial Poisson Equation Approach discussed above and the new results are shown in the following figures.
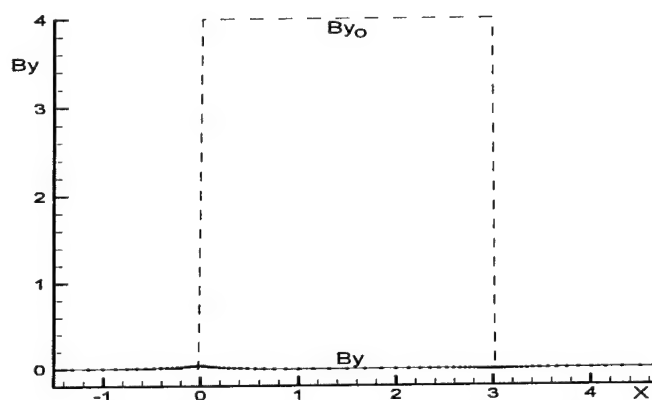
Figure 18. Solution for $\mathbf{B_y}$ along centerline.

Notice that B_y now increases at x=0, where previously it decreased, as shown in Fig.13.

Figure 19. Solutions for $\mathbf{E_z}$ along centerline.

Fig.19 reveals a really shocking surprise. The $\mathbf{E_z}$ solution to the MFD equations, with the constraint on the divergence of the magnetic field maintained, adjusts toward the original imposed magnetic field $\mathbf{E_{z0}}$, and not the solution E'_z to the "Equation for E_z" of Subsec.6.3 given earlier.
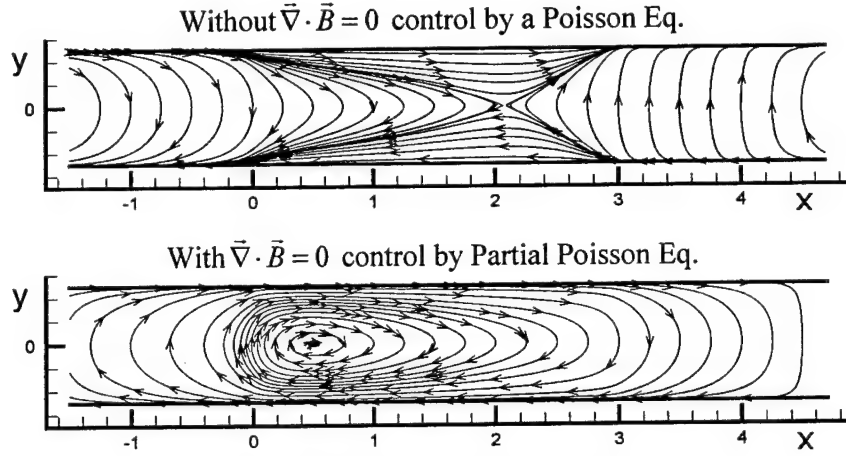
Figure 20. Magnetic Field Lines

The magnetic field lines for both sets of results are shown in Fig.20. The results of Sec.6.5 did not use a Poisson Equation to maintain a divergence free magnetic field and the results of the present section used a Partial Poisson Equation for control. Note the large difference in the field line distributions. The top figure resembles a supersonic wave pattern in the electrode region while the lower figure appears to be like streamlines for a slowly rotating flow.

7. Analysis of Non-Uniqueness of the Equations of Magneto-Fluid Dynamics (Item (8) in the Status of Effort Section above).

Two solutions have been presented for the extended accelerator geometry test problem. Is either solution correct? Both satisfy the MFD equations and boundary conditions. Compare the solutions for E_z in Fig.14 with that in Fig.19. To say that the latter solution is correct because it satisfies $\vec{\nabla} \cdot \vec{B} = 0$ is not sufficient. The first solution agrees with the solution E'_z to the "Equation for E_z" of Subsec.6.3 and the latter adjusts toward the original imposed magnetic field $\mathbf{E_{zo}}$. We can determine which is correct by looking at the unsteady Ampere-Maxwell Equation.

$$\frac{\partial \vec{E}}{\partial t} = \frac{1}{\varepsilon_e}\left(\frac{\vec{\nabla} \times \vec{B}}{\mu_e} - \vec{J} \right)$$

But an underlying assumption made in deriving the MFD Equations is $\quad \vec{J} = \frac{1}{\mu_e}\vec{\nabla} \times \vec{B}$

Hence, $\dfrac{\partial \vec{E}}{\partial t} = 0$ and $E_z = E_{zo}$ is the correct solution. It satisfies the unsteady Ampere-Maxwell Equation as well as the constraint $\vec{\nabla} \cdot \vec{B} = 0$.

The velocity and $\mathbf{B_y}$ fields are shown in Fig.21 and Fig.22.
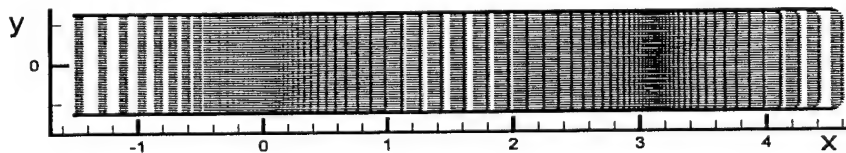
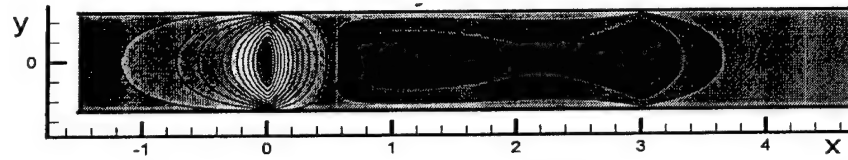**Figure 21.** Velocity Field , With $\vec{\nabla} \cdot \vec{B} = 0$ control

Figure 22. B_y Field., With $\vec{\nabla} \cdot \vec{B} = 0$ control
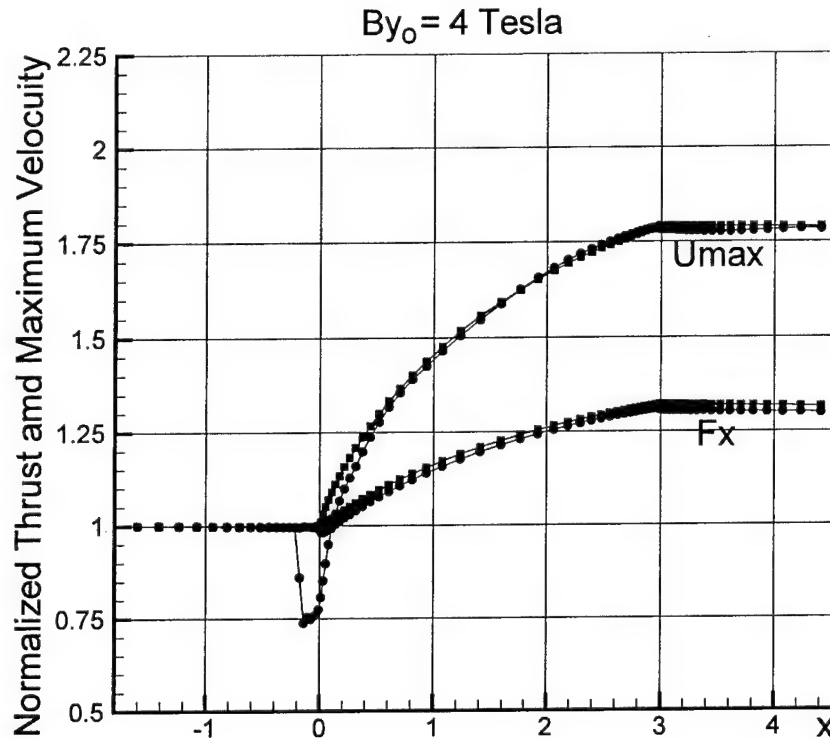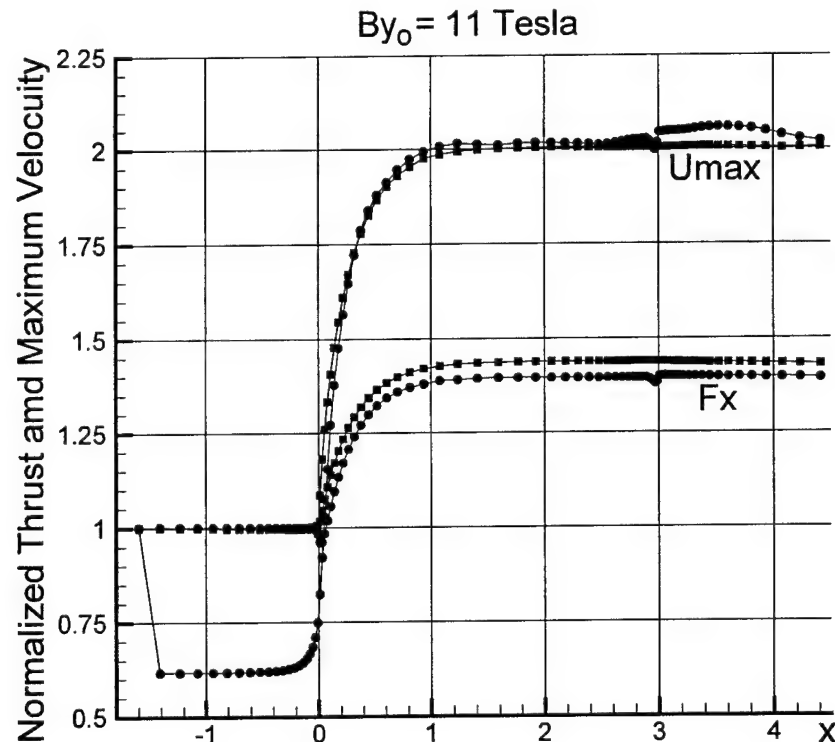

Figure 23. Comparison of Full MFD and Low Re Approaches (red squares) for Normalized Thrust and Maximum Velocity with B_{yo}=4 T.

Fig.23 compares the Full MFD and Low Magnetic Reynolds Number Approaches for predicting thrust and maximum velocity within the accelerator. At B_{yo}=4 Tesla the two approaches agree very well. However, note the velocity disturbance near x=0 in the Full MFD results. It appears that a shock wave is propagating upstream toward the boundary. Further inspection did show the presence of a shock wave moving upstream. The Low Magnetic Reynolds Number Approach did not and could not show a similar feature. The question is – Should this shock wave be physically present or not? Did it start out from numerical difficulties produced by the strong discontinuity in the imposed magnetic field? The calculation was repeated using as the initial solution the converged solution from Low Magnetic Reynolds Number Approach. The shock wave reappeared.

A second test case was simulated with a stronger magnetic field. The imposed magnetic field was $B_{yo} = 11$ Tesla and the electric field was $E_{zo} = -30,000$ V/m., again with the same load factor of 2.004. All other conditions were unchanged.

Figure 24. Comparison of Full MFD and Low Re Approaches (red squares) for Normalized Thrust and Maximum Velocity with B_{yo}=11 T.

Fig.24 compares the Full MFD and Low Magnetic Reynolds Number Approaches for predicting thrust and maximum velocity within the accelerator. Again, the presence of a strong shock is observed. It has moved to the upstream boundary. There are significant differences in thrust predicted by the two approaches. At present, from further testing, it is believed that the Low Magnetic Reynolds Number Approach is incorrect and, at these conditions, a shock wave does move upstream toward the entrance boundary.

8. Inclusion of Cesium Seeding into the Flow and the Park Model for Calculating Electrical Conductivity Based upon Electron and Ion Concentrations (Item (9) in the Status of Effort Section above).

Previously a numerical difficulty was discussed in Sec.2 concerning the Park program for calculating electrical conductivity near the wall within the boundary layer. This difficulty is now removed by finding and correcting a statement in the Park program. Simulation results were then made for a non-equilibrium flow.

An experimental Magneto-Hydrodynamic (MHD) channel is being tested at NASA Ames Research Center by D.W. Bogdanoff, C. Park and U.B. Mehta to study critical technologies related to MHD bypass scramjet propulsion. The channel about a half meter long contains a nozzle designed for Mach 2 flow, a center channel section and an accelerator section. Magnetic and electric fields can be imposed upon the flow within accelerator section for MHD acceleration. The channel was uniformly 2.03cm wide.
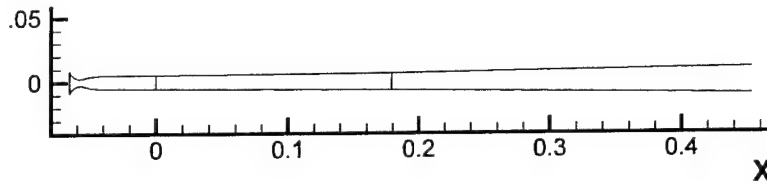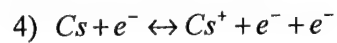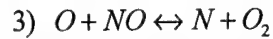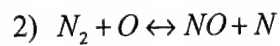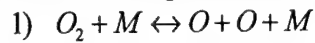
Figure 25. NASA MHD Channel experiment

The initial conditions for the nozzle section consisted of the flow at rest at $8.0 \times 10^5 \mathrm{N/m^2}$ pressure, $7500°\mathrm{K}$ temperature and an exit pressure low enough to generate supersonic flow. Because of flow symmetry only half the channel was simulated in this 2-D calculation.

The imposed magnetic field was $B_y = 4$ Tesla and the electric field was $E_z = -25,000$ V/m. The gas in the accelerator was seeded and considered to be in non-equilibrium. The following four reaction seeded air chemistry model of Park, Mehta and Bogdanoff was used. The model contains eight species.

$$1) \quad O_2 + M \leftrightarrow O + O + M$$

$$2) \quad N_2 + O \leftrightarrow NO + N$$

$$3) \quad O + NO \leftrightarrow N + O_2$$

$$4) \quad Cs + e^- \leftrightarrow Cs^+ + e^- + e^-$$

The electrical conductivity was calculated from the species mole fractions, temperature, density and pressure of the gas, using a program developed by Park. A Baldwin-Lomax turbulence model modified for MFD was used.
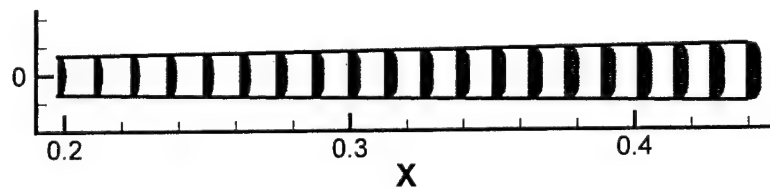

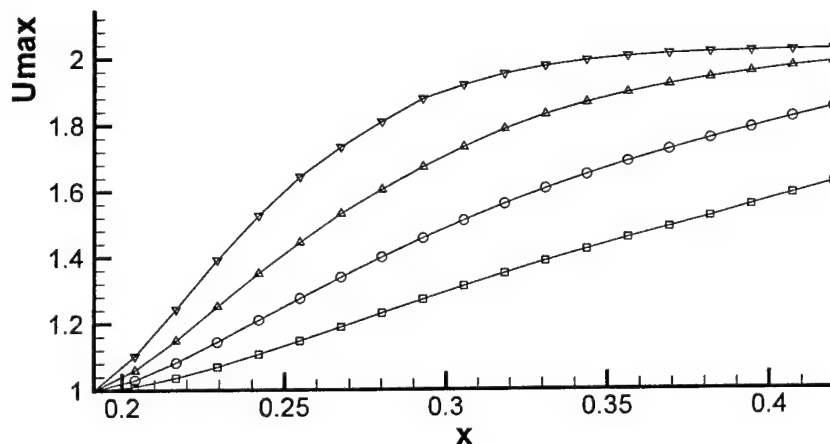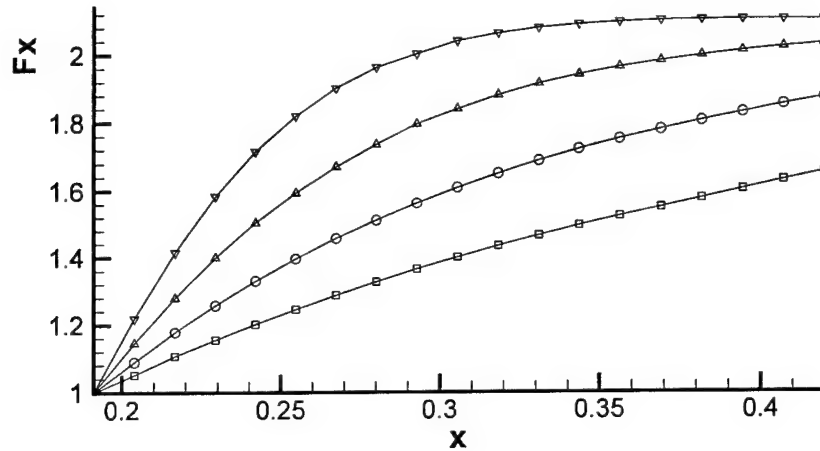**Figure 26**. Velocity profiles, 2-D accelerator

Figure 27. Maximum velocity in the axial direction within accelerator section for initial Cs concentrations of 0.3, 0.6, 1.2 and 2.4×10^{-3}

**Figure 28.** Normalized force in the axial direction within accelerator section for initial *Cs* concentrations of 0.3, 0.6, 1.2 and 2.4x10^{-3}

Fig.25 shows the acceleration of velocity within the channel and Fig.26 and Fig.27 show the increase in both axial velocity and force with increasing seeding concentrations of *Cs*. Earlier reported difficulties in solving this problem have been overcome.

9. Analysis of the Physics of Upstream Influence of the Flow about the Nose of a Hypersonic Vehicle Concentrations (Item (10) in the Status of Effort Section above).

A preliminary study on the upstream influence of the hypersonic flow about a sphere cone body simulating the flow about the nose of a hypersonic vehicle has been started. We observed the importance of the upstream influence of flow governed by the equations of magneto-fluid dynamics earlier within channels simulating the flow in generators and accelerators relevant to the "energy bypass scramjet engine concept". Now we examine external hypersonic flow. Fig.29 shows "Mach One" contour about a sphere cone body immersed in Mach 15 flow. The cone half angle is 15 degrees. The Mach One contour was calculated by dividing the velocity normal to the body surface by the speed of sound and locating values of unity . It is essentially the location of the bow shock wave about the body, but not exactly so, and separates the flow disturbed by the body from the free stream.
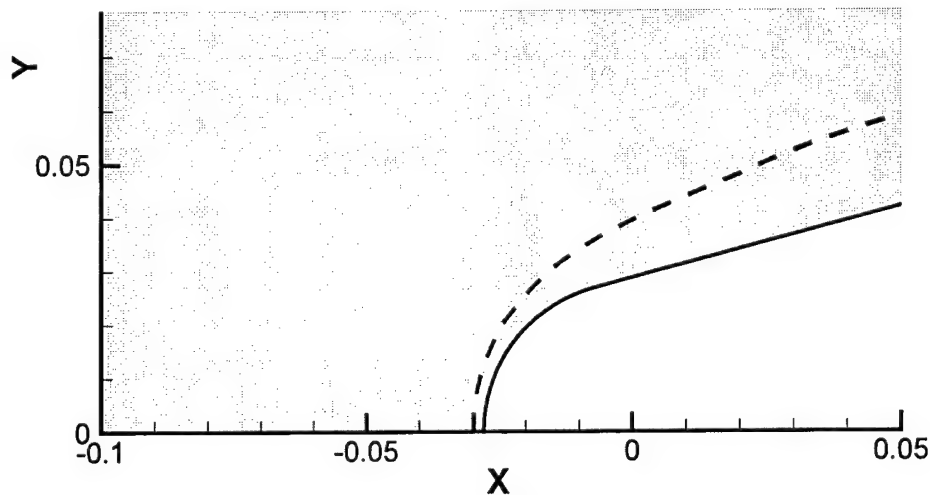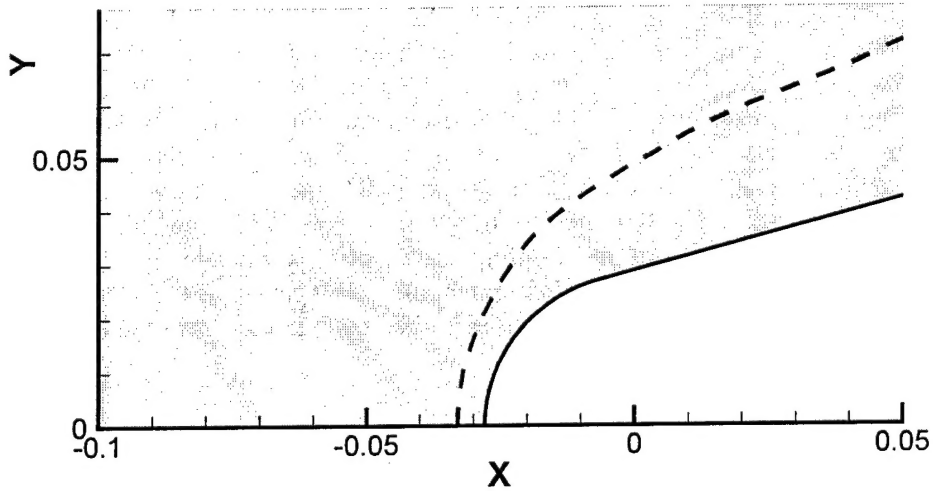

Figure 29. Mach One contour location, $|v_n / c|$, no magnetic field
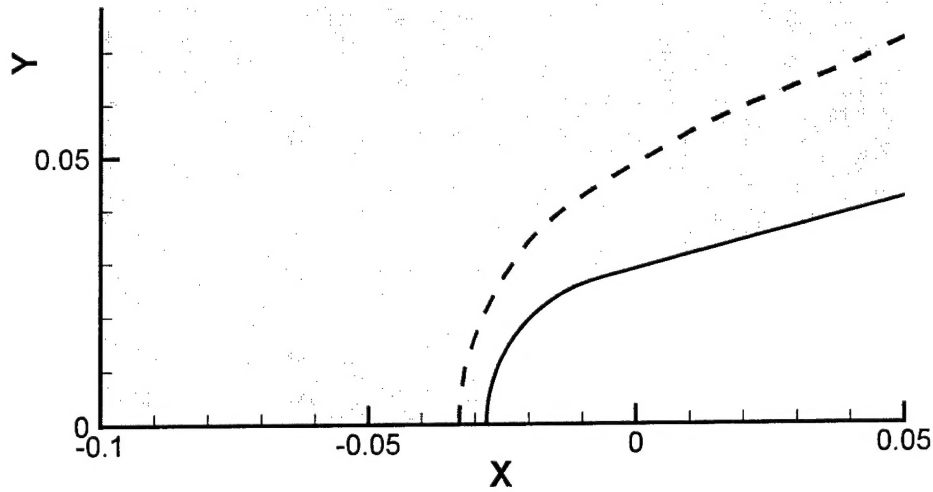
Figure 30. Mach One contour location, $\left| v_n / c \right|$, Interaction Parameter $Q = \sigma_e B_o^2 l_0 / \rho_0 u_0 = 6$, Full MFD Equations

Fig.30 shows the Mach One contour location with a magnetic dipole placed at the origin. Note the increased standoff distance. Fig.31 shows the same flow calculated by the Low Magnetic Reynolds Number Approach. The agreement of the Full MFD and Low R_m MFD Equations is excellent.
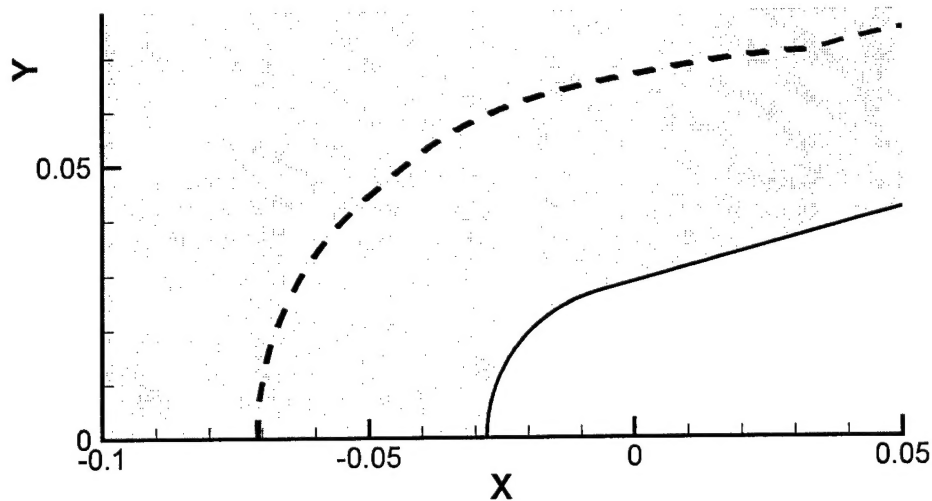

Figure 31. Mach One contour location, $\left| v_n / c \right|$, Interaction Parameter $Q = \sigma_e B_o^2 l_0 / \rho_0 u_0 = 6$, Low R_m MFD Equations

Fig.32 shows the Mach One contour using the "fast sound speed" c_f instead of the usual speed of sound c.

$$c_f = \sqrt{\frac{1}{2}\left(c^2 + \frac{B^2}{\rho} + \sqrt{\left(c^2 + \frac{B^2}{\rho}\right)^2 - 4c^2 \frac{B_x^{\,2}}{\rho}}\right)}$$

Magnetic fields can propagate small disturbances with speed c_f, which can be many times larger than

c. The sound speed c_f is directional. That given above is for the x-direction of travel.

Figure 32. "Fast "Mach One contour location, $\left|v_n/c_f\right|$, Interaction Parameter $Q = \sigma_e B_o^2 l_0 / \rho_0 u_0 = 6$, Full MFD Equations

Note the greatly extended region of disturbed flow described by the Full MFD Equations. This extended region would not occur from the Low R_m MFD Equations because there are not other modes of wave propagation than the usual sonic speed.

An important question is "what is happening in the extended region?'. It appears that the flow is slowly compressing and heating up until it passes over the bow shock wave where suddenly jumps up in pressure, density and temperature. Thus, the region just ahead of the bow shock is not undisturbed free stream flow, but flow with a higher temperature than that of the free stream. Hence, the Mach number just ahead of the bow shock wave is reduced from the free stream Mach number. It is amazing that the Low R_m MFD Equations miss this entirely yet still predict the bow shock location accurately. But, are there other important features of the flow that the Low R_m MFD Equations fail to predict? It appears that the heating of the flow outside of the shock wave may have a significant effect of body surface heat transfer. This will be explored subsequently.

10. Importance of this Research
This research has pointed out the simulation differences between the Full MFD and Low Reynolds Number Equation approaches. The former is a very complicated set of equations, with non-uniqueness issues and constraint satisfaction difficulties. However, it is a more complete description of the flow about and through bodies of Air Force interest than the simpler Low Reynolds description, now in widespread use. The present status in the development of algorithms for the equations of magneto-fluid-dynamics is not yet mature enough to simulate flows about aerospace configurations with confidence. It is important to continue this research to avoid catastrophic design errors caused by flow simulations that do not include all the relevant physics.

Personnel Supported:

Name	Degree	Discipline	Involvement
MacCormack, R.W.	M.Sc.	Aeronautics and Astronautics	50%
Suh, Joo	Graduate student	Aeronautics and Astronautics	100%
Murphy, M.	Graduate student	Aeronautics and Astronautics	100%

Publications:

☒

1) MacCormack, R.W., "Three Dimensional Plasmadynamics Algorithm Development," *AIAA Paper No. 2002--0197*, 2002, 40th Aerospace Science Meeting, Reno NV, January 2002.

2) MacCormack, R.W., "Three Dimensional Plasmadynamics Calculations," *AIAA Paper No. 2002--2162*, 2002, 33rd Plasmadynamics and Lasers Conference, Maui, HI, 23-26 June 2002.

3) MacCormack, R.W., ``Three Dimensional Plasmadynamics - Flow Field Calculations," *AIAA Paper No. 2003--0325*, 2003, 41st Aerospace Science Meeting, Reno NV, January 2003.

☒

4) MacCormack, R.W., ``☒Flow Calculations with Strong Magnetic Fields," *AIAA Paper No. 2003--3623*, 2003, 34th Plasmadynamics and Lasers Conference, Orlando, FL, 23-26 June 2003.

5) MacCormack, R.W., "Flow Calculations with Strong Magnetic Effects," *AIAA Paper No. 2004--0318*, 2004, 42nd Aerospace Science Meeting, Reno NV, January 2004.

6) MacCormack, R.W., "Magneto-Aerodynamic Flow Calculations with Strong Magnetic Fields," *AIAA Paper No. 2004--2163*, 2004, 35th Plasmadynamics and Lasers Conference, Portland, OR, June 2004.

Interactions/Transitions:
Previous versions of the developed numerical procedures have been transitioned to NASA Ames Research Center, and Georgia Tech. and Wright State Universities. The present version will be available for transition soon.

Research interactions have been made with the following
Dr. Suresh Menon , Georgia Tech
Dr. U. Mehta, NASA Ames Research Center
Dr. D. Gaitonde, AFRL/VA
Prof. J. Shang, Wright State University

Presentations
R.W. MacCormack
  40th AIAA Aerospace Science Meeting, January 2002
  33rd Plasma Dynamics & Laser Conference, June 2002
  41st AIAA Aerospace Science Meeting, January 2003
  34th Plasma Dynamics & Laser Conference, June 2003
  42nd AIAA Aerospace Science Meeting, January 2004
  35th Plasma Dynamics & Laser Conference, June 2004

Inventions, or Patent Disclosures:
None

Honor/Awards:
 No new honors or awards